

# First Test Flight Thermal Performance of the Low Density Supersonic Decelerator (LDSD) Supersonic Flight Dynamics Test (SFDT) Vehicle

A. J. Mastropietro<sup>1</sup>, Jason Kempenaar<sup>1</sup>, Matthew Redmond<sup>1</sup>, and Michael Pauken<sup>2</sup>  
*Jet Propulsion Laboratory, California Institute of Technology, Pasadena, California, 91109*

*and*

Walt Ancarrow  
*WCA Engineering, Inc., Jarrettsville, Maryland, 21084*

The first of three planned experimental flights of the Low Density Supersonic Decelerator (LDSD) Supersonic Flight Dynamics Test (SFDT) vehicle took place on the morning of June 28<sup>th</sup>, 2014 off the coast of Kauai, Hawaii. The goal of the first flight was to determine if the vehicle could reach the altitudes and airspeeds needed to test new technologies for decelerating supersonic vehicles destined for Mars. SFDT-1 was launched from the Navy's Pacific Missile Range Facility (PMRF) on a 960,000 cubic meter helium carrier balloon provided by NASA's Columbia Scientific Balloon Facility (CSBF). Once lifted to a stable float altitude of 36.4 km over the Pacific Ocean, the vehicle was dropped and a series of automated maneuvers began. First, the vehicle was spun up via small rocket motors to provide trajectory stability and then a third stage Star 48 solid rocket motor fired to accelerate the vehicle up to Mach 4.3 at an altitude of 54.2 km. After main engine burnout, the vehicle was spun down with another set of small rockets and testing of the new deceleration system in Mars analogous conditions began. A 6-meter doughnut shaped Supersonic Inflatable Aerodynamic Decelerator (SIAD-R) was successfully deployed around the test vehicle and performed flawlessly, slowing the vehicle to about Mach 2.5 before the second technology was deployed – an enormous Supersonic Disk Sail Parachute (SSDS) that had more than double the area of the most recent parachute used to land Curiosity. The parachute, however, did not inflate properly but it provided enough drag to allow the vehicle to survive a water impact largely intact. Despite the parachute anomaly, the test was still hailed as a success, and the engineering team is using all of the recovered vehicle hardware and data recorders to learn how to improve upon the technology for subsequent test flights scheduled in 2015 and 2016. The vehicle's thermal control system effectively protected the avionics, batteries, cameras, data recorders, and composite core structure during both the cold ascent and powered flight which posed a high heating environment. The thermal telemetry from the first test flight, an assessment of post-flight inspections of the recovered vehicle, and a review of the thermal design and model of the vehicle will be presented along with several lessons learned.

## Nomenclature

<i>AFT</i>	= Allowable Flight Temperature
<i>CRD</i>	= Command Receiver Decoder
<i>CSA</i>	= Core Structure Assembly
<i>CSBF</i>	= NASA Columbia Scientific Balloon Facility
<i>DCC</i>	= Drop Circuit Controller

---

<sup>1</sup> Thermal Systems Engineer, Thermal and Fluids System Engineering Group.

<sup>2</sup> Senior Thermal Systems Engineer, Thermal and Fluids System Engineering Group.

<i>DVR</i>	= Digital Video Recorder
<i>EPSU</i>	= Ethernet Power Switching Unit
<i>FIR</i>	= Flight Image Recorder
<i>GG</i>	= Gas Generator
<i>GLNMAC</i>	= Gimballed LN-200 with Miniature Airborne Computer (IMU)
<i>GPS</i>	= Global Positioning System
<i>HR</i>	= High Resolution
<i>HS</i>	= High Speed
<i>HST</i>	= Hawaiian Standard Time
<i>IMU</i>	= Inertial Measurement Unit
<i>JPL</i>	= NASA Jet Propulsion Laboratory
<i>LDSD</i>	= Low Density Supersonic Decelerator
<i>LNA</i>	= Low Noise Amplifier
<i>MSFC</i>	= NASA Marshall Spaceflight Center
<i>NASA</i>	= National Aeronautics and Space Administration
<i>PCM</i>	= Pulse Code Modulation
<i>PDD</i>	= Parachute Deployment Device
<i>PMRF</i>	= U. S. Navy Pacific Missile Range Facility
<i>PSM</i>	= Power Supply Module
<i>RF</i>	= Radio Frequency
<i>SFDT</i>	= Supersonic Flight Dynamics Test
<i>SIAD-E</i>	= Supersonic Inflatable Aerodynamic Decelerator, Exploration Class
<i>SIAD-R</i>	= Supersonic Inflatable Aerodynamic Decelerator, Robotic Class
<i>SSD</i>	= Solid State Disk (within FIR)
<i>SSDS</i>	= Supersonic Disk Sail Parachute (tested during SFDT-1)
<i>SSRS</i>	= Supersonic Ring Sail Parachute (original baselined parachute – old nomenclature)
<i>TM</i>	= Telemetry
<i>TPS</i>	= Thermal Protection System
<i>TV</i>	= Test Vehicle
<i>UTC</i>	= Coordinated Universal Time
<i>WFF</i>	= NASA Wallops Flight Facility
<i>WRA</i>	= Water Recovery Aid
<i>XMTR</i>	= Transmitter

## I. Introduction

NASA's Low Density Supersonic Decelerator (LDSD) Project is developing three new aerodynamic braking devices in order to land heavier payloads at higher elevations on Mars than is currently possible with the heritage Viking era technology<sup>1-5</sup>, which was last used for landing the 1 ton Curiosity rover in 2012. As shown in Fig. 1, two of the drag augmenting mechanisms under development are Supersonic Inflatable Aerodynamic Decelerators (SIADs) and the third is a new 30.5 meter diameter Supersonic Disk Sail (SSDS) parachute. The robotic class SIAD-R consists of a compressed gas inflated torus with a total diameter of 6 meters upon deployment around the Supersonic Flight Dynamics Test (SFDT) vehicle. The SIAD-E variant for the exploration class of missions is intended to inflate to an 8 meter diameter isotensoid using a combination of compressed gas and ram air. The first stratospheric test flight of the SFDT vehicle configured with a SIAD-R successfully took place on the morning of June 28, 2014 after launching

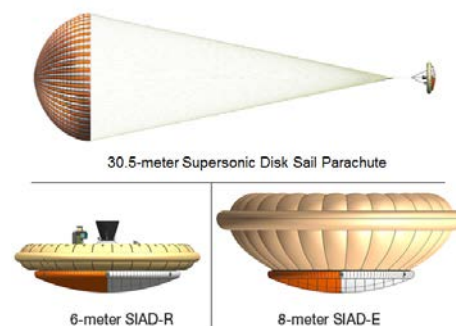


**Figure 1.** The LDSD project will develop and test two sizes of inflatable aerodynamic drag devices and a large new supersonic disk sail parachute using the SFDT vehicle in a series of high altitude flight tests<sup>6</sup>.

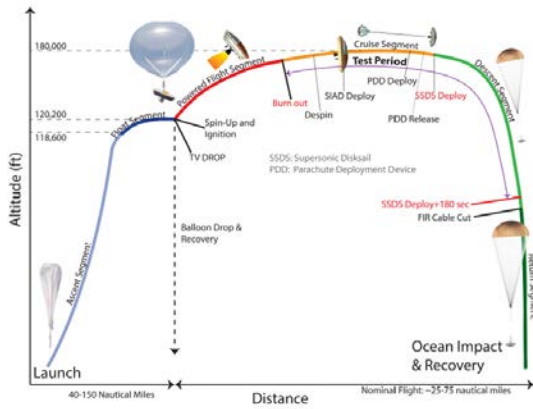


**Figure 2. Flight profile for high altitude LDS test in Earth's stratosphere using the SFDT vehicle.**

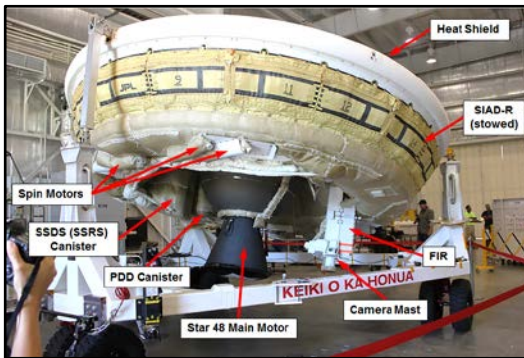


**Figure 3. Flight ready Test Vehicle #1 at PMRF.**



**Figure 4. SFDT vehicle suspended from the launch tower.**

from the Navy's Pacific Missile Range Facility (PMRF) Kauai, Hawaii<sup>7</sup>.

Figure 2 shows the intended flight profile for this stratospheric test which is supposed to briefly simulate a Mars-like entry environment while the decelerators are implemented. A large helium carrier balloon provided by NASA's Columbia Scientific Balloon Facility (CSBF) lifts the SFDT vehicle to a stable float altitude of about 118,000 ft (36 km) where it is then dropped, spun up for inertial stability using small rocket motors, then boosted up to an altitude of about 180,000 ft (55 km) and a speed of approximately Mach 4 using a Star 48 rocket motor, and finally despin, ready to deploy the technologies under development. The SIAD is inflated around the aeroshell to dramatically increase the drag surface area and reduce the vehicle speed to approximately Mach 2. Afterwards, a Parachute Deployment Device (PDD), comprised of a mortar and a ballute, subsequently pulls the 30.5 m SSDS parachute out of the vehicle to complete the vehicle deceleration sequence and ultimately return the vehicle back to the ocean where recovery operations can begin.

Many details on the development of the SFDT vehicle, SIADs, and parachute can be found in Refs. 8-12. This paper touches on a brief review of the thermal design and analysis of the SFDT vehicle, and then focuses primarily on the thermal performance of the SFDT vehicle during its first flight test.

## II.SFDT Flight Test #1 Objectives

The first SFDT flight was intended as a shakeout flight of the entire test architecture. The minimum success criteria were declared by the project as the following<sup>13</sup>:

1. Launch the SFDT vehicle with a Star-48 on a balloon from PMRF to float altitude.
2. Conduct a powered flight, demonstrating the ability to target Mars analogous Mach numbers and dynamic pressures.
3. Collect real-time telemetry from the test vehicle sufficient to assess the powered flight objective and to demonstrate the operation of all radio links.
4. Recover the balloon from the ocean for disposal.

Since the first SIAD-R and SSDS elements were ready ahead of time enabling integration with SFDT-1, secondary goals were established as the following:

- Deploy and collect data on the operation and dynamics of the SIAD-R.
- Deploy and collect data on the operation and dynamics of the SSDS parachute.
- Fly the camera mast assembly and other SIAD and SSDS sensors.
- Recover the test vehicle and/or flight image recorder from the ocean.

### III. SFDT Vehicle Description, Mission Timeline, and Day of Test Thermal Environment

The ready-for-flight SFDT-1 vehicle is shown in Fig. 3. The primary elements of the vehicle are a Composite Core Structure Assembly (CSA), a Heat Shield, a Camera Mast, a Star 48 Main Motor, Spin Motors, and the stowed decelerator technologies to be tested – a SIAD-R, and a combined PDD/SSDS system. The Wallops Flight Facility (WFF) provided avionics pallet and the GLNMAC Inertial Measuring Unit (IMU) which are embedded in one of the 6 internal bays of the vehicle are best seen in Figs. 9-11.

At 08:00 HST on June 28, 2014, SFDT-1 was powered on for launch. Figure 4 depicts the vehicle on the launch tower ready for balloon launch. During this time, the carrier balloon was being inflated off to the side of the tower, and once it was ready, it was released and allowed to float over the top of the tower at which time the tower then released the vehicle initiating launch at 08:40 HST. Table 1 summarizes the time stamps for the critical events of the mission which followed with an emphasis towards those that have thermal performance ramifications while Fig. 5 displays the corresponding ground track of the entire test flight which occurred off the west coast of Kauai.

In order to understand the aerodynamic behavior of the test vehicle, knowledge of the atmospheric density and speed of sound throughout the anticipated flight regime is required. For SFDT-1, various weather balloons and meteorological rockets were launched around the timeframe of actual SFDT operations in order to fully characterize the temperatures of the atmosphere at lower and upper altitudes. The left hand side of Fig. 6 displays the reconstructed as-measured temperature profile vs. altitude mostly bracketed by the worst case thermal analysis assumptions. It is apparent that the Model Hot Case assumptions were not entirely bounding between the altitudes of 40km and 45km. On the right hand side of Fig. 6, the interpolated mission time vs. atmospheric sink temperature is plotted. The Model Cold Case had assumed launch would occur in the dark before sunrise, whereas Flight 1 actually launched about 40 minutes later in the morning than was originally thought permissible. When all three curves are shifted to coincide with balloon launch, it can further be observed that the worst case cold ascent rate was also not thoroughly bounding. The earlier portion of the ascent was in reality much faster than assumed. This is important to capture correctly in the future so the maximum time spent within the coldest part of the troposphere is properly accounted for.

Overall SFDT-1 was a significantly faster mission than had been thermally analyzed. The actual mission phase elapsed times for SFDT-1 were as follows (worst case hot analytical discrepancies noted):

- Pre-Launch Power Up – 41 minutes (vs. 30 minutes modeled)
- Ascent – 2 hours 21 minutes (vs. 2 hour 45 minutes modeled)
- Float – 3 minutes (vs. 3 hour 15 minutes modeled)
- Drop to SSDS Full Inflation – 2 minutes 49 seconds (vs. 3 minutes modeled)
- Descent to Splash Down – 17 minutes (vs. 35 minutes modeled)

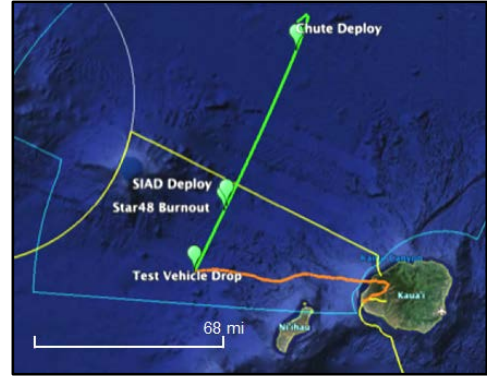


Figure 5. Balloon and test vehicle ground tracks after launch from PMRF in Kauai.

Table 1: SFDT Flight #1 Critical Event Time Stamps on June 28, 2014

Critical Event	UTC	HST
Pre-Lift Check Begins	12:02:00	2:02:00
Pre-Lift Check Complete	12:32:00	2:32:00
Post Lift Check Begins	15:47:00	5:47:00
Post-Lift Check Complete	16:05:00	6:05:00
Pre-Launch Power ON	18:00:00	8:00:00
Balloon Launch	18:40:51	8:40:51
Balloon Rotator ON	20:05:53	10:05:53
Balloon Rotator Set	20:18:59	10:18:59
TV Block 1 Power ON	20:25:10	10:25:10
TV Block 2 Power ON	20:30:07	10:30:07
TV Block 3 Power ON	20:35:37	10:35:37
TV Block 4 Power ON	20:50:14	10:50:14
Float Achieved	21:02:47	11:02:47
GLNMAC Init	21:03:01	11:03:01
Drop	21:05:00	11:05:00
Spin Up	21:05:00	11:05:00
Star 48 Ignition	21:05:02	11:05:02
Star 48 Burnout Detected	21:06:11	11:06:11
Spin Down	21:06:12	11:06:12
SIAD Deploy	21:06:22	11:06:22
PDD Mortar Fire	21:07:41	11:07:41
SSDS Full Inflation	21:07:49	11:07:49
FIR Cable Cut	21:10:53	11:10:53
EPSU Altitude Switch Closure	21:19:20	11:19:20
All Buses Powered OFF	21:19:32	11:19:32

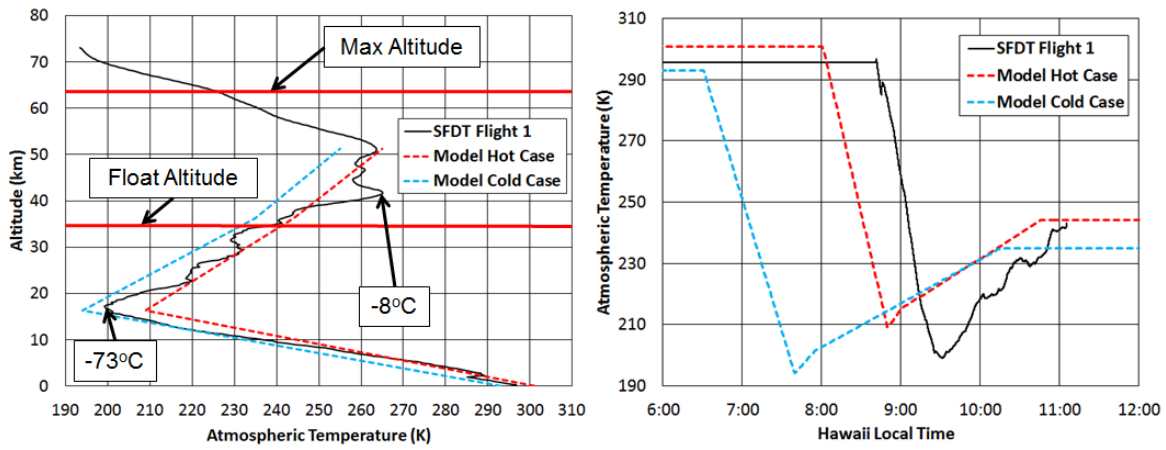


Figure 6. Reconstructed atmospheric temperature profile for SFDT-1 on June 28, 2014 with comparison to thermal model bounding cases.

#### IV. Brief Review of SFDT Thermal Design and Thermal Model

Reference 14 provides details on the bounding LDS thermal analysis assumptions, environments, and the Thermal Desktop<sup>®</sup> model shown in Fig. 7 that was developed to support the thermal design of the SFDT vehicle. The thermal subsystem design passively protects the vehicle structure and its components from the cold temperatures experienced during the ascent phase of the mission as well as from the extreme heat fluxes imposed during the supersonic test phase by the Star 48 Main Motor, Spin Motors, and from aerothermal heating. Additionally, the thermal design safely rejects all of the onboard avionics power dissipation in order to maintain components within their allowable flight temperatures (AFTs). This passive thermal design approach for the SFDT vehicle relied upon careful and complex bounding analysis of all three modes of heat transfer – conduction, convection, and radiation – coupled with a tightly managed transient power dissipation timeline for the onboard electronics throughout all mission phases. Early on, the avionics pallet required considerable thermal redesign in order to enable the mission. The avionics had to be laid out carefully, high emittance coatings had to be used wherever possible to maximize the radiative heat rejection, and the individual component’s power on times had to be minimized whenever possible in the mission timeline. Figure 8 is intended to give the reader a flavor of the thermal model results which shows the worst case hot analysis temperature profiles for the avionics pallet. As mentioned, this was a very fast mission compared to what was thermally analyzed. During SFDT-1 the first drop attempt was successful vs. the three drop attempts modeled in the worst case hot profile. Descent to splash down should have nominally lasted about 35 minutes as well, but was expedited due to the chute failure. If the SSDS had remained intact, many components would have stayed on for a bit longer and reached higher temperatures than the flight telemetry shows.

There were really four major challenges which were worrisome from the standpoint of the vehicle thermal control and that had design implications which rippled across

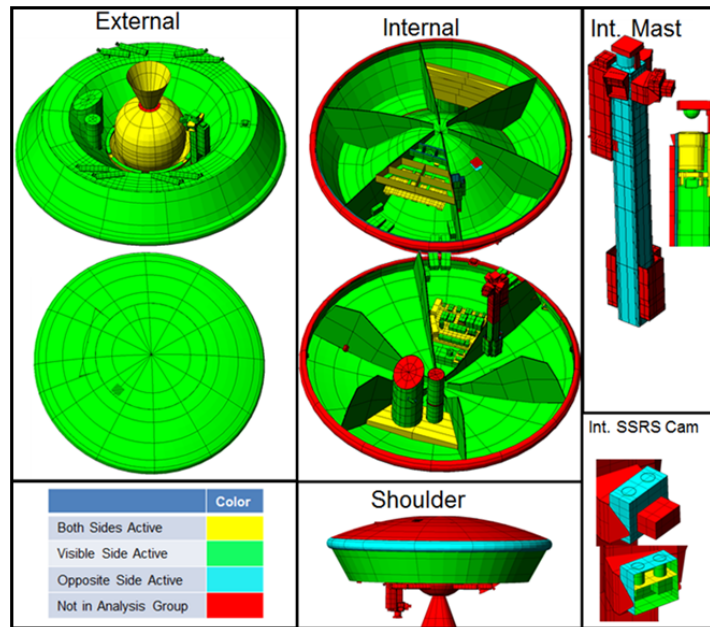


Figure 7. The SFDT Thermal Desktop Model<sup>®</sup> with various radiation analysis groups displayed.

the entire flight system. All of the following four challenges had been estimated by third parties to be significantly high heating events:

1. Star 48 Main Motor plume heating
2. Star 48 Main Motor soakback heating
3. Spin Motor plume heating
4. Spin Motor soakback heating

Reference 15 addresses some of the concerns revolving around the Spin Motor plume and soakback heating and Ref. 16 delves into the effort to find low cost candidate materials for the TPS layups needed to help address these thermal challenges.

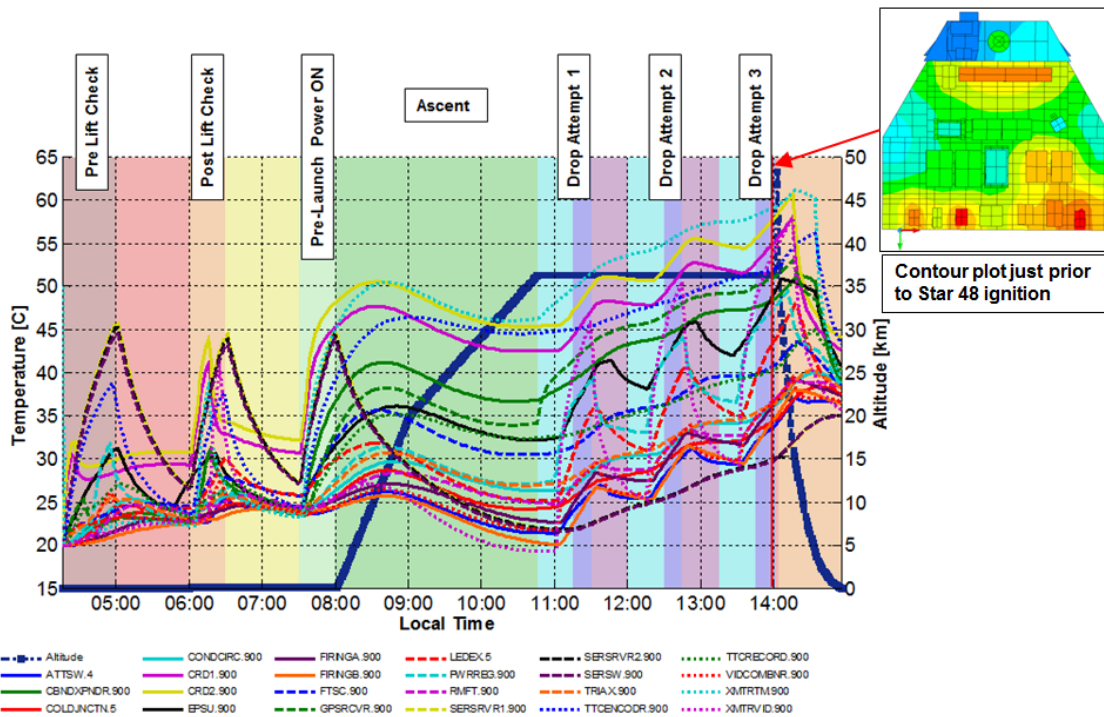


Figure 8. Avionics pallet worst case hot analysis results with 3 drop attempts assumed (refer to Fig. 11)

## V. SFDT-1 Thermal Telemetry and Thermal Performance Assessment

Figures 9-15 convey the vehicle layout and specify the names and locations of all the onboard thermal sensors. The names of each of the channels are fairly self-descriptive. Flight day telemetry for 136 out of the 145 existing flight temperature channels is plotted in Figs. 16-45 from pre-launch power up until altitude shutdown on Saturday, June 28, 2014. 1 sensor on Battery #2 was declared non-functional prior to launch and 7 sensors were not connected (2 situational video cameras on the camera mast, and 5 internal 1-wire sensors for the main batteries). 3 sensors were likely not behaving properly – *TH\_P\_FIRINGB*, *TC\_SIAD\_B7LEE*, and *TC\_SIAD\_C8GAS*. There was only 1 in-flight operating AFT violation – with 2 sensors near the nozzle of the Star 48 falling below the minimum AFT of +7°C for the solid propellant for about 1 hour before warming back up to within limits prior to the Main Motor firing. The minimum qualification limit for the propellant was never violated. The thermal performance of the various elements of the vehicle is discussed in more detail below.

### A. Batteries (See Figs. 9, 10, 16, & 17)

There are 6 thermal sensors for measuring the cell temperatures of the 5 main batteries (Li-MnO<sub>2</sub>) and 1 drop battery (NiCd) as shown in Fig. 9. Additionally, there were 5 battery fuse temperature sensors for each of the main batteries as shown in Fig. 10. Note that the fuses were located in separate compartments attached to the side of each battery pack. Unfortunately, the *TH\_BATT2\_CELL* channel was not functional for SFDT-1. The main battery cells AFTs were +10°C to +60°C and despite their large mass, they were actually predicted to get too cold if they were simply mounted within the SFDT vehicle without any consideration for thermal control. Thus, the packs that the cells were contained in were eventually wrapped with a low emittance tape to more effectively isolate them from the surrounding environment. Figures 16 and 17 show the benign thermal telemetry that was collected for the batteries and their fuses. Note the fuses had much wider AFTs of -25°C to +75°C, although they all remained between +23°C and +37°C.

### B. Avionics Pallet Components (See Figs. 8-11, & 18-23)

The avionics pallet temperature sensors include 14 external thermistors, 8 cold junction stack thermocouples, and 15 internal board temperature sensors. Figure 18 shows that the Telemetry (TM) Transmitter which was left on continuously throughout the entire mission remained the hottest component on the pallet reaching a peak temperature of +53°C towards the end of the flight. This limit was well under its maximum worst case hot predict of +61°C as seen in Fig. 8 (refer to curve labeled *XMTRTM.900*). Before it was turned on later in the flight, the Video Transmitter was observed to be the coldest component on the pallet at +21°C. This result was good confirmation that the pallet thermal layout was optimal since the transmitters which were anticipated to be two of the hottest avionics components were purposely mounted on the part of the pallet that had the best radiative view to the colder Heat Shield in order to ensure maximum heat rejection. After it was turned on, the video transmitter indeed became the second hottest component on the pallet peaking at about +47°C. Despite its continuous operation, the third hottest component was the Pulse Command Modulator (PCM) Encoder which stayed just below +40°C as shown in Fig. 20. After the TV Blocks #1-4 power on, the Command Receiver Decoder (CRD), the Global Positioning System (GPS) unit, and the Power Regulator all peaked near +37°C. Note how the CRD was originally warmer than the PCM Encoder prior to balloon launch. After approximately 30 minutes into the ascent, the CRD cools off well below the PCM Encoder due to its more optimal position between the transmitters on the pallet where more effective radiative heat rejection occurs as previously mentioned.

Figures 19, 22, and 23 depict several critical internal avionics board temperatures that were also recorded during Flight #1. After TV drop occurred, the EPSU, Power Regulator, Firing Circuit A, and Firing Circuit B internal

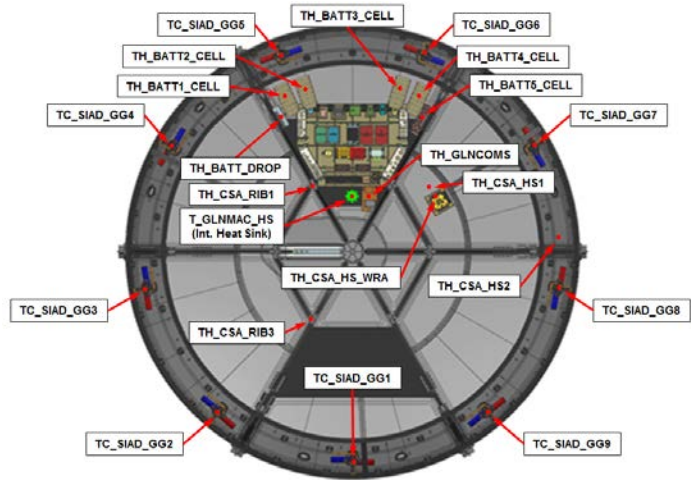


**Figure 9.** Temperature sensor locations for main and drop batteries, GLNMAC and GLN-Coms, core structure Heat Shield and ribs, and SIAD gas generators. Avionics pallet is also shown in the same bay that batteries and GLNMAC reside in.

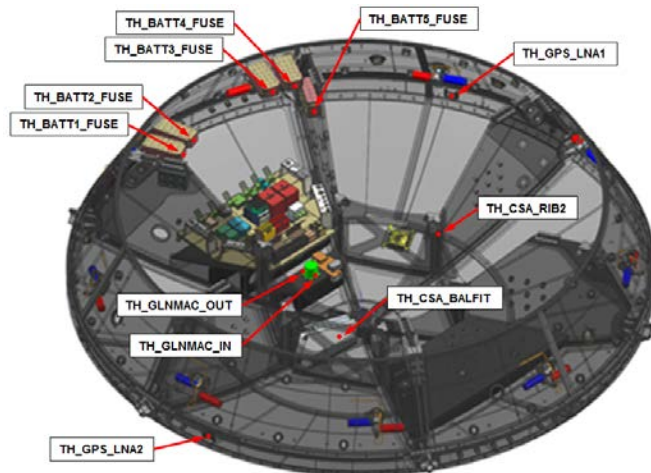


**Figure 10.** Temperature sensor locations for main batteries fuses, GPS LNAs, GLNMAC, and core structure balloon fitting and rib.

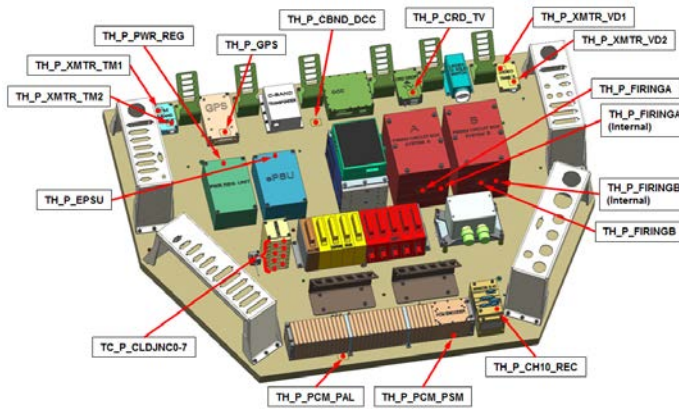


**Figure 11. Avionics pallet temperature sensor locations.**

the coldest at +29°C. After TV drop, it was a relief to witness that there was little to no increased temperatures observed on any of the pallet components due to the effect of the Main Motor plume heating followed by its soakback heating, indicating that the pallet was effectively insulated from these events. All pallet mounted avionics stayed well within their AFTs.

### C. GLNMAC (See Figs. 9, 10, 24, & 25)

During flight operations, special thermal attention was given to the GLNMAC in particular due to it having a fairly restrictive internal temperature limit and a marginal thermal design that relies principally upon radiative heat transfer from its housing that is mounted to a composite shelf via thermally and mechanically isolating rubber grommets. Also, its suboptimal position within the vehicle sandwiched between two significant sources of additional heating – the avionics pallet and the Main Motor – further highlighted the need for increased operational scrutiny.

Thus, the GLNMAC temperature telemetry collected consists of a total of 2 external thermistors as shown in Fig. 10, and 12 internal temperature sensors that were only available when GLNMAC was powered on. In addition, because the telemetry from the 12 internal temperature channels was not directly piped to the thermal operator in real time, 1 more internal channel ( $T_{GLNMAC\_HS}$ ) was implemented as a real time proxy for the internal *Gimbal Heatsink* channel.

All 15 channels of the GLNMAC thermal telemetry are plotted in Figs. 24 and 25. The GLNMAC was powered on 15 minutes prior to drop in order to minimize its power on time. This decision reflected the appropriate balance of risk in terms of mitigating the GLNMAC from getting too hot during multiple drop attempts while still providing adequate time prior to drop to ensure that it was properly initialized for the powered flight.

The internal limiting component, the *Optical Rx*, reached +40.4°C after approximately 30 minutes of continuous power on time and was increasing at a rate of 0.4°C/min prior to altitude shutdown. At this time, the external case temperature as shown in Fig. 24 peaked at +36.9°C and lagged behind the *Optical Rx* by only 3.5°C. In the worst case for Flight 1, the GLNMAC was expected to be on for 70 minutes continuously while accounting for a hold. Assuming the 0.4°C/min ramp rate had remained constant, the *Optical Rx* would have reached +57°C (safely under its +61°C qualification limit) had it remained on for the full 70 minutes. No increased temperatures were observed on any of the GLNMAC temperature channels due to the effect of the Main Motor plume heating followed by its soakback heating, affirming that the GLNMAC was effectively shielded from these events.

Based upon the thermal telemetry, it's likely that the GLNMAC could tolerate approximately 80 minutes of continuous operation at altitude with its internal temperature still remaining under the +61°C qualification limit. However, in order to ensure the *Optical Rx* stays below this limit, it's still recommended that the total power on time for GLNMAC be conserved to the extent possible. While turning off the GLNMAC in flight would prevent its temperature from continuing to rise, ground testing confirmed it's not likely to cool off quickly because it is thermally isolated from the surrounding structure.

Lastly, during the TV trajectory stabilization spin, the GLNMAC internal *Gimbal Heatsink* channel did not rapidly rise in temperature due to the spinning gyro inside the LN-200 as some previous sounding rocket flight test

boards peaked at temperatures of +57°C, +53°C, +45°C, and +36°C, respectively. These temperatures were considered to be extremely benign. Figure 19 also shows that the externally box mounted Firing B thermistor was reporting suspect temperatures for most of the mission. It should have mimicked the Firing A thermistor much more closely. After the Ordnance A and B buses were powered on, it seems that the misbehaving thermistor started to sense more representative temperatures. When the vehicle was dropped, there was approximately a 23°C degree gradient observed across the components mounted on the pallet with the TM Transmitter being the hottest at +52°C, and the Thermocouple (TC) Cold Junction stack being

data indicated would happen. In fact, there were no noticeable changes in any of the GLNMAC temperature ramp rates during this phase of the mission.

#### D. GPS Low Noise Amplifiers (LNAs) (See Figs. 10 & 26)

There is 1 temperature sensor for each GPS LNA on the SFDT vehicle as shown in Fig. 10. The LNAs are mounted on metal brackets on the interior perimeter of the core structure in the vicinity of the L-band antenna patches. The temperatures observed during SFDT-1 are presented in Fig. 26. Initially, while powered off, the LNAs cooled down during the ascent to about +6°C. After the Sensor Bus was powered on, they warmed up to at a rate of approximately 0.3C/min but remained well within their AFTs of -30°C to +61°C.

#### E. Cameras, CoreDVRs, and FIR (See Figs. 3, 12, & 27-29)

The camera mast as shown in Figs. 3 and 12 contains 3 situational video cameras which monitor the Spin Motor firings, as well as the SIAD, PDD, and SSDS deployments, 1 high speed panoramic machine vision camera for viewing the SIAD deployment, and 2 more machine vision cameras – 1 high speed and 1 high resolution – solely for viewing the PDD and SSDS deployments. The machine vision cameras recorded their data utilizing a 3 unit CoreDVR system positioned at the bottom of the mast which collected and stored the data on 12 Solid State Disks (SSDs) mounted within a shock resistant, detachable buoyant housing positioned further up the mast called the Flight Image Recorder (FIR).

There are 8 available thermistors in total on the camera mast, 1 each for the CoreDVRs, 3 for only the cameras which view the PDD and SSDS deployments, 1 for the panoramic SIAD viewing camera, and 1 for the SSDs. In addition, there is one more situational video on the top deck that has a thermistor. This camera overlooks the Main Motor firing as well as the very early portion of the PDD and SSDS deployments. All of the cameras were packaged within insulated housings that were designed to provide sufficient thermal mass to ride out the intense plume heating from the Main Motor burn while simultaneously conducting away internally dissipated heat via metallic mounting interfaces from the camera bodies. Each camera also had a retractable protective lens cover to shield the detectors during the Main Motor firing and to mitigate any soot build up that might otherwise obstruct their views.

The temperatures for all of the camera equipment are plotted in Figs. 27-29. As shown in Fig. 27 the plume facing cameras did realize some increased temperatures due to the Main Motor plume heating, although not as much as was predicted. The most pronounced effect was observed on Situational Video Camera #4 which experienced about a 9°C increase in temperature due to the Main Motor plume heating event. While significant, the camera mast thermal design overall appears to have been very robust since all camera mast equipment remained well inside AFTs.

Note the CoreDVRs had to be repackaged from their commercial off the shelf configurations since they were designed to be convectively cooled via fans in air at sea level. More thermally efficient voltage regulators were implemented, and all of the internal hot components were re-mounted so as to enable cooling by conduction and radiation only, thereby allowing them to function in a near vacuum environment. The CoreDVRs peaked at around 30°C after drop but remained within their AFTs of -10°C to +55°C.

The FIR housing was designed to promote conductive cooling from the internally dissipating SSDs to the surrounding structure which was also insulated against the heat pulses from both the Main Motor and Spin Motor

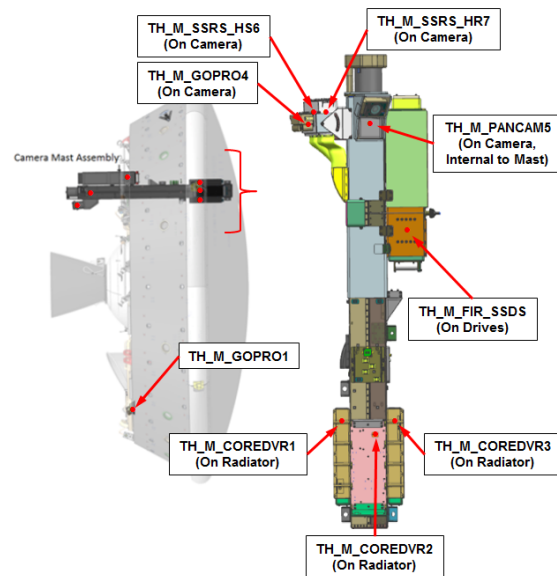
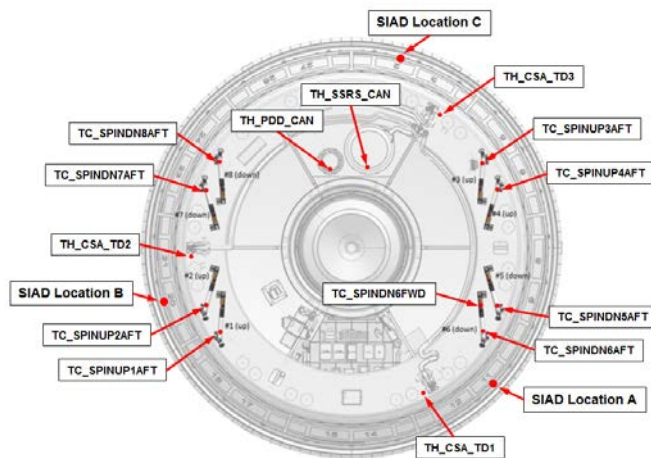


Figure 12. Camera system temperature sensor locations.

firings with exterior layers of cork. The in-flight temperature of the FIR SSDs as shown in Fig. 29 remained quite benign and well inside its AFTs of  $-40^{\circ}\text{C}$  to  $+50^{\circ}\text{C}$ .



**Figure 13. Spin Motor, parachute system, top deck, and SIAD (reference next figure) temperature sensor locations.**

sufficient vaporization pressure at the critical time, the aqueous methanol mixture must be at an elevated temperature to ensure that there is adequate internal energy available.

It was a goal to have the Inflation Aid above  $+40^{\circ}\text{C}$  when the rupture disk bursts. To achieve this, heaters were bonded to the outer wall of the PDD canister and the Inflation Aid was heated indirectly through the packed ballute surrounding it. These heaters were powered only through ground support equipment, and were not active during launch preparation and the subsequent flight. Thus, the Inflation Aid had to be heated well above the desired  $40^{\circ}\text{C}$  to be at this temperature 16-18 hours after the heater was disconnected. Ground testing and thermal analysis confirmed that the Inflation Aid needed to be heated to  $80^{\circ}\text{C}$  which could only be achieved after more than 30 hours of continuous heating prior to launch due to the low thermal diffusivity of the enclosed system.

For SFDT-1, the PDD canister was heated for over 36 hours prior to heater disconnect in order to warm the Inflation Aid up to  $80^{\circ}\text{C}$ . Given the observed PDD canister flight temperatures in Fig. 30, the Inflation Aid was likely at  $43^{\circ}\text{C}$  when it was implemented after only 12 hours of cooling, leading to a highly successful ballute deployment.

### G. Core Structure Assembly (See Figs. 9-11, & 31-33)

The composite core structure AFTs were  $-48^{\circ}\text{C}$  to  $+74^{\circ}\text{C}$ . Figures 9-11 show the various locations of all of the Composite Structure Assembly (CSA) thermistors. There are 2 thermistors on the Heat Shield inner facesheet in the camera mast bay, 1 on the Water Recovery Aid (WRA) that protrudes through the Heat Shield, 1 on the metallic balloon fitting, 3 on the ribs immediately underneath the Main Motor adaptor outer ring, and 3 on the top deck underneath the TPS. The majority of the aft structure was protected by a fiberglass and alumina mat TPS construction. The forebody was protected from the aerodynamic heating imposed during supersonic flight by a cork Heat Shield, and the Main Motor was mounted on a steel conical adaptor mounting flange that was designed to provide sufficient thermal isolation from the composite structure. Temperatures for all these areas were quite benign as shown in Figs 31-33, and demonstrate a robust thermal design. Note much of the TPS insulation once implemented was actually considerably thicker than prescribed in many of the critical regions, and may have contributed to the extremely benign temperatures of the underlying structures it served to protect.

### F. Parachute(Inflation Aid/PDD/SSDs) (See Figs. 3, 13, & 30)

The SSDs (SSRS) and PDD canisters sit side by side on the vehicle as shown in Figs. 3 and 13. One thermistor is on each of the cans underneath the TPS. The PDD is deployed first followed by the SSDs. The PDD relies on an internal Inflation Aid to assist with the initial ballute pressurization. After the mortar firing event and once the PDD bag is at line stretch, a pyrotechnic initiator causes a rupture disk to burst and expel an aqueous methanol mixture from the Inflation Aid canister into the attached ballute vessel. The mixture immediately vaporizes and provides the initial pressure boost needed to puff up the ballute and allow its ram air inlets to complete the inflation process.

In order for the Inflation Aid to provide

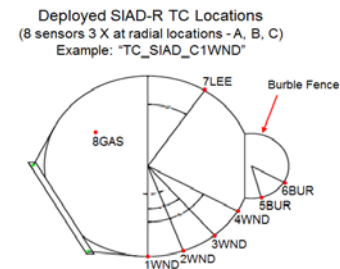


**Figure 14. Deployed SIAD-R temperature sensor locations (reference previous figure).**

## H. Spin Motors (See Figs. 3, 13, 34, & 35)

As shown in Fig. 13, each Spin Motor had a Type K thermocouple near its nozzle precisely located on the motor wall where one edge of the solid propellant grain was in close proximity. Only Spin Down Motor #6 had two thermocouples bonded to it in an attempt to capture the axial gradient between opposite ends of the fired motor. It's important to mention that the numbering of the Spin Motors was unrelated to their actual firing order. In fact, the firing Spin Up pair order was #1& #3 simultaneously, then #2 & #4, followed by Spin Down Motors #6 and #8, and finally #5 & #7. Figure 34 shows that Spin Motor temperature gradients between firing pairs prior to drop were on the order of 2°C, well under the allowable 19°C total dispersion (beyond which it was feared that uneven Spin Motor thrusting was more likely to develop undesirable nutation). Figure 35 shows all Spin Motors experienced a mild rise in temperature after they were fired with initial temperatures between +7°C and +15°C, and the soakback into the core structure was likely insignificant despite the preliminarily concerning estimates.

## I. Main Motor (See Figs. 3, 15, 36, & 37)

Figure 15 shows the position of all 8 thermocouples on the Star 48 Main Motor. 4 thermocouples were on the forward dome, 2 were on the mid-section, and 2 thermocouples were on the aft end of the Star 48 Main Motor near the nozzle. Figure 36 shows that the 2 aft sensors reached about +1°C which was slightly colder than the minimum solid propellant AFT of 7°C and remained below this limit for about an hour while ascending through the cold portion of the troposphere before naturally warming back up to within limits prior to Main Motor firing. It's not likely that the propellant actually experienced this cold temperature excursion because an insulation liner exists between the titanium motor casing and the propellant which would produce a significant temperature gradient. Furthermore, there is not any solid propellant in the immediate vicinity of the aft sensors. There was an additional concern that the nearby Star 48 Safe and Arm Device might have gotten too cold, but real time discussions during operations confirmed that it was qualified to -51°C and it too turned out to be a non-issue. Immediately after the Main Motor burnout, the forward dome experienced significant soakback heating as shown in Figure 37 with temperatures peaking at 282°C. As was mentioned previously, the heat pulse to the supporting core structure underneath appears to have largely been mitigated since no temperature rise was witnessed on the nearby ribs. Post-flight inspection also revealed that there was minimal slag in the forward dome, a finding which was again counter to prevailing thought prior to the first flight. The possibility of a considerable amount of hot slag in the forward dome did force the team to come up with a robust solution for thermally isolating the entire Star 48 from the rest of the vehicle with sturdy TPS blankets and a heavy steel motor adaptor mount.

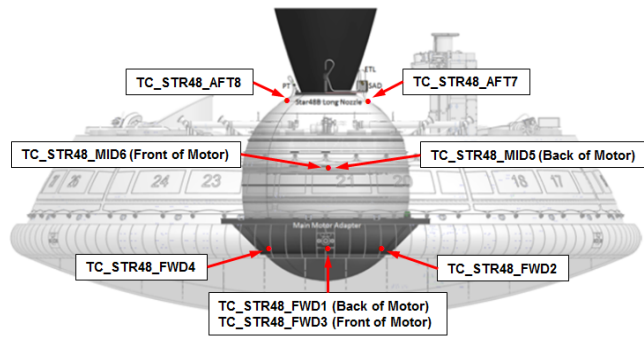


Figure 15. Star 48 Main Motor temperature sensor locations.

## J. SIAD (See Figs. 3, 9, 13, 14, & 38-45)

The SIAD-R was instrumented with 24 thermocouples, with 8 per the radial locations identified in Figs. 13 and with nomenclature as defined in Fig. 14. The SIAD gas generators were similarly instrumented around the perimeter of the vehicle as shown in Fig. 9. All of the collected SIAD thermal telemetry is plotted in Figs. 38-45. Note that one SIAD sensor in each radial location was supposed to be suspended within the inflated pressure vessel so that it could capture the internal gas temperature. It appears that 2 channels – *TC\_SIAD\_B7LEE* and *TC\_SIAD\_C8GAS* – may have been misbehaving since their signatures were markedly different from the other locations. Just prior to chute inflation, the externally mounted sensors at Locations A and B peaked at ~120°C while location C peaked at less than 100°C, after which they all cooled off dramatically during the rapid descent. These peak temperatures are

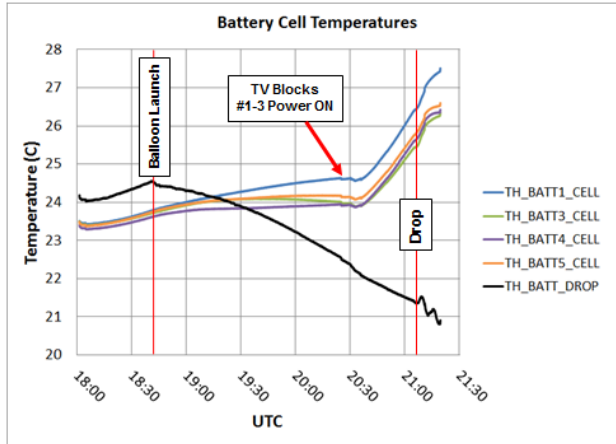


Figure 16. Main and drop batteries temperatures (Battery #2 thermistor was not functional for Flight #1).

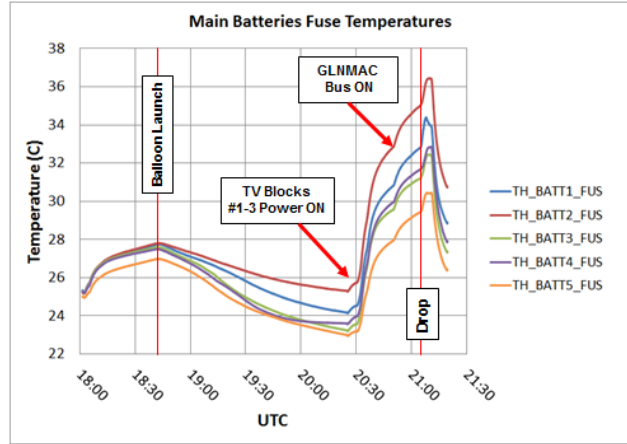


Figure 17. Main batteries fuse temperatures (fuses are located separately from cells within each battery pack).

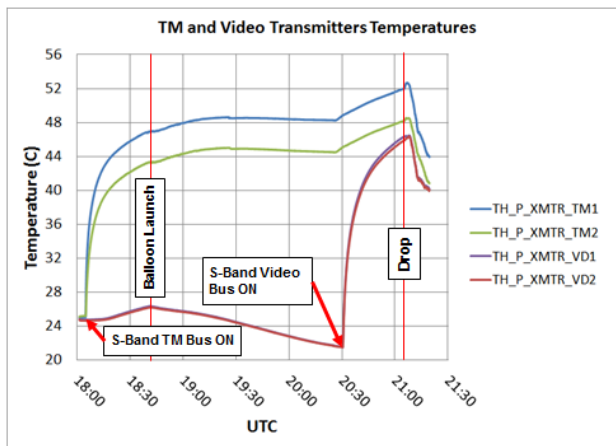


Figure 18. Telemetry (TM) and video transmitter temperatures. Vid xmtr turned on 35 min before drop.

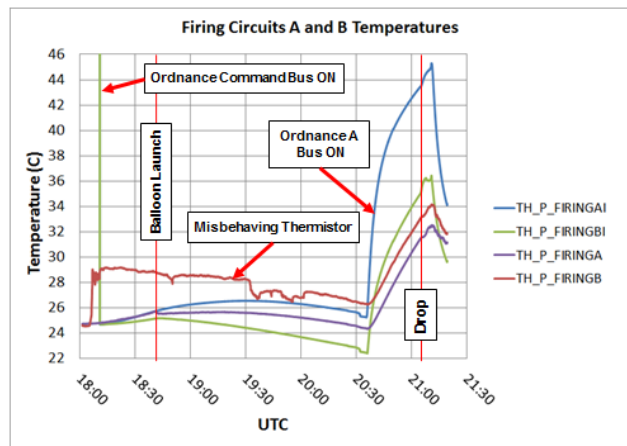


Figure 19. Firing circuits temperatures. Firing B sensor should have mimicked Firing A sensor more closely.

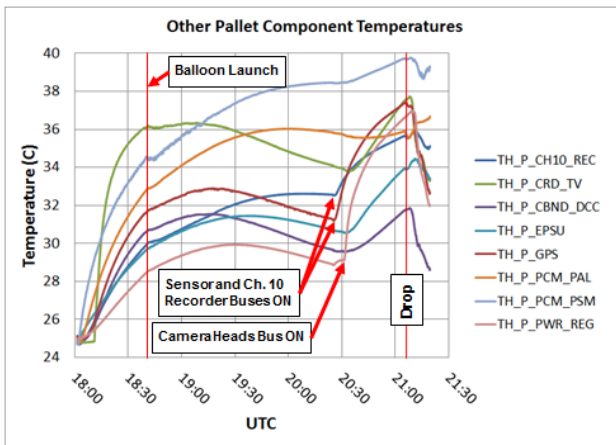


Figure 20. Temperatures of majority of components on pallet.

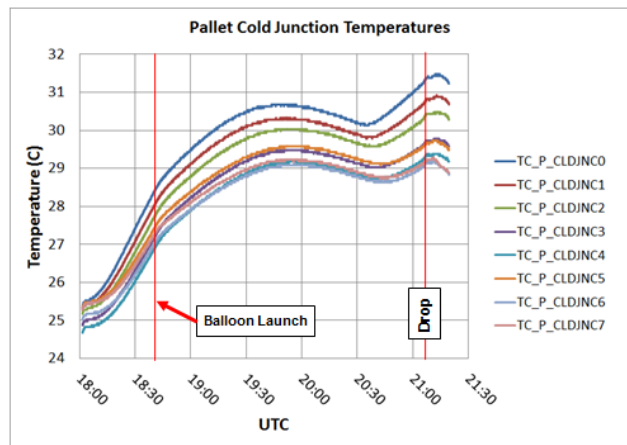


Figure 21. Cold junction thermocouple stack temperatures on pallet.

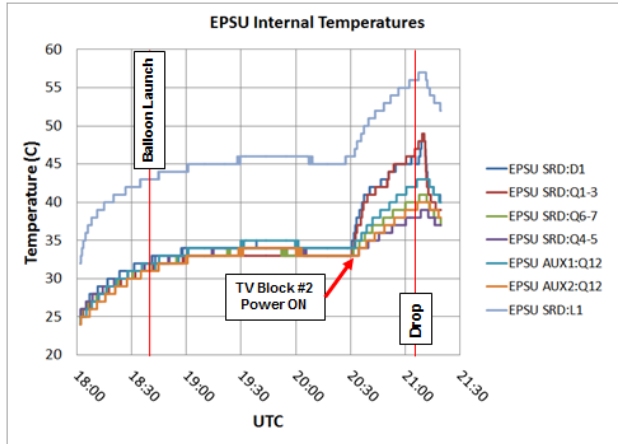


Figure 22. EPSU internal board temperature telemetry.

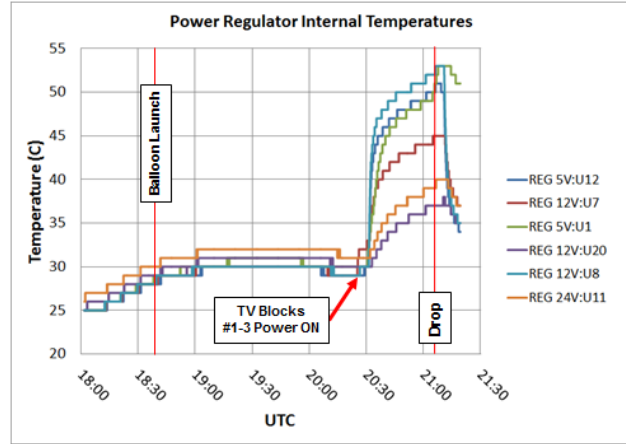


Figure 23. Power Regulator internal board temperature telemetry.

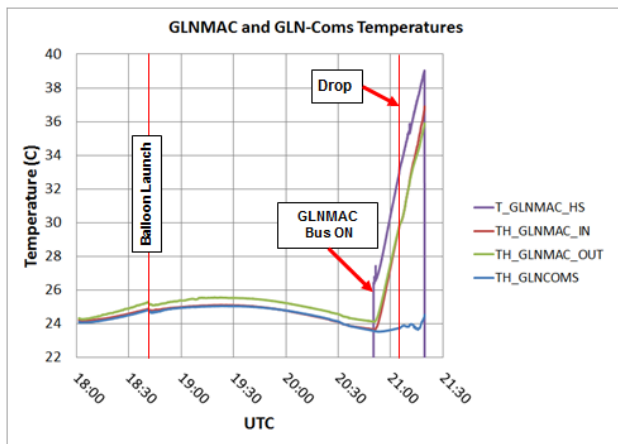


Figure 24. GLNMAC and GLN-Coms temperatures.

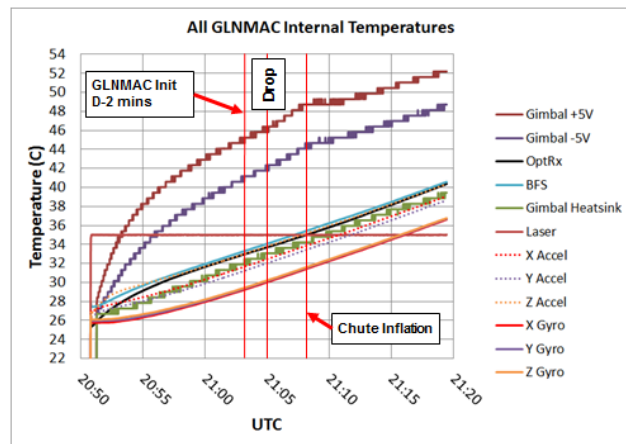


Figure 25. GLNMAC internal temperatures during operation. Optical Rx peaked at 40°C.

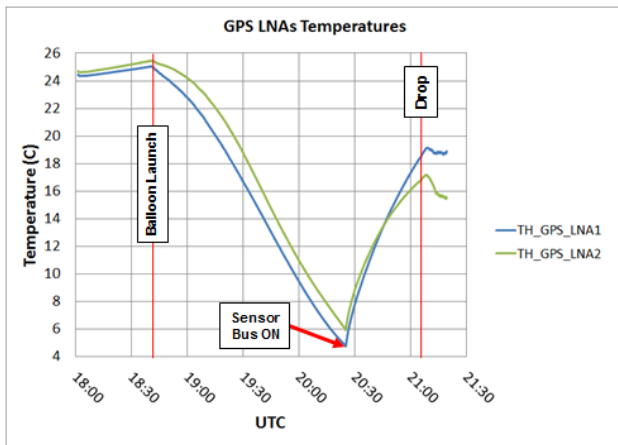


Figure 26. GPS Low Noise Amplifiers (LNAs) temperatures.

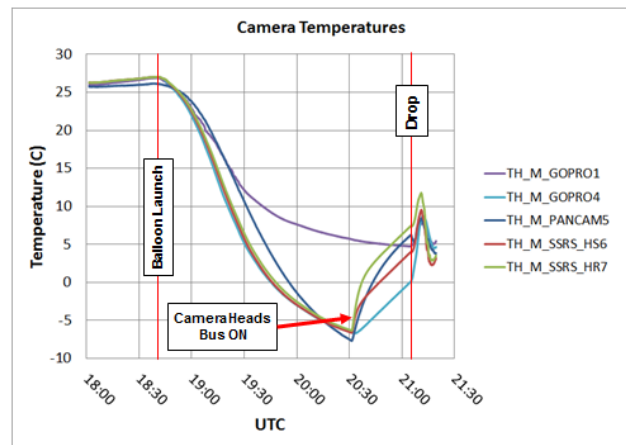


Figure 27. Machine Vision/Situational Video camera temperatures.

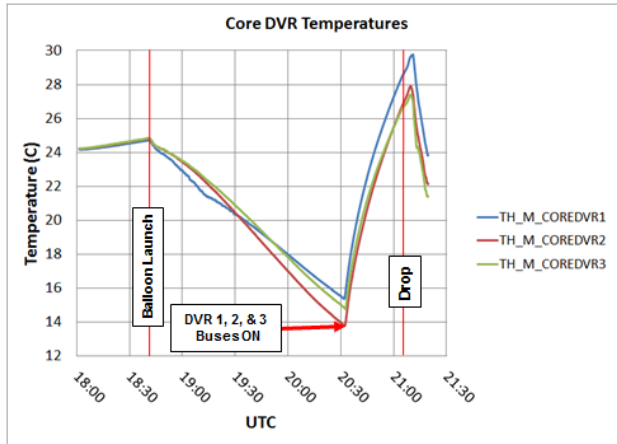


Figure 28. Core DVR temperatures.

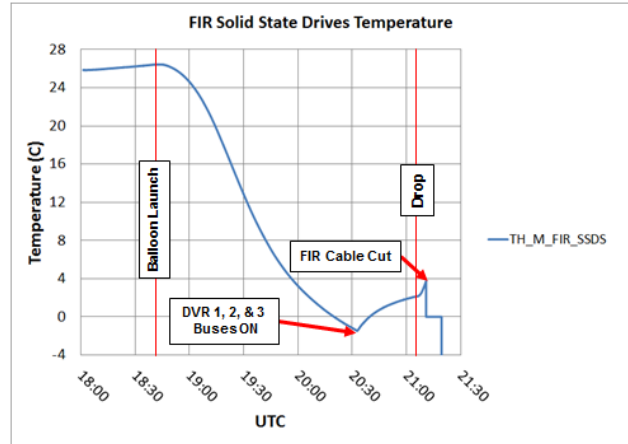


Figure 29. Flight Image Recorder (FIR) Solid State Disks temperatures. Cable cut after chute deployed.

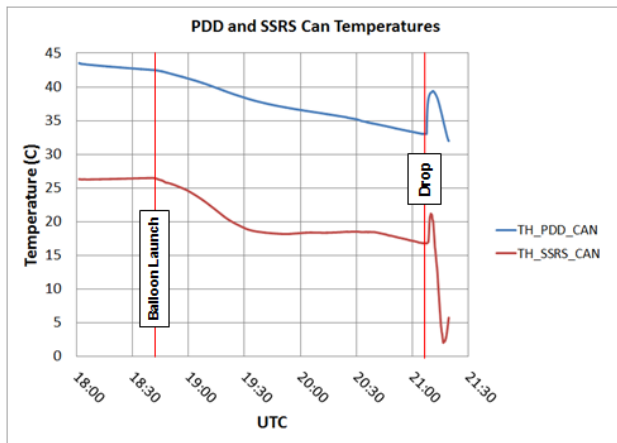


Figure 30. PDD and SSRS Canister temperatures. Inflation Aid within PDD canister likely at 44°C prior to deployment.

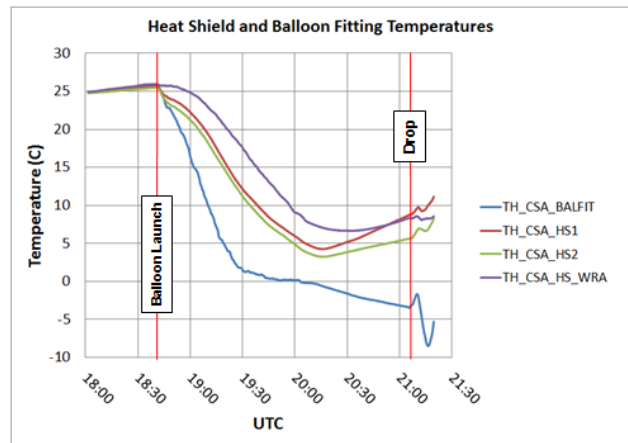


Figure 31. Heat Shield inner facesheet, Heat Shield Water Recovery Aid (WRA), and Balloon Fitting temperatures.

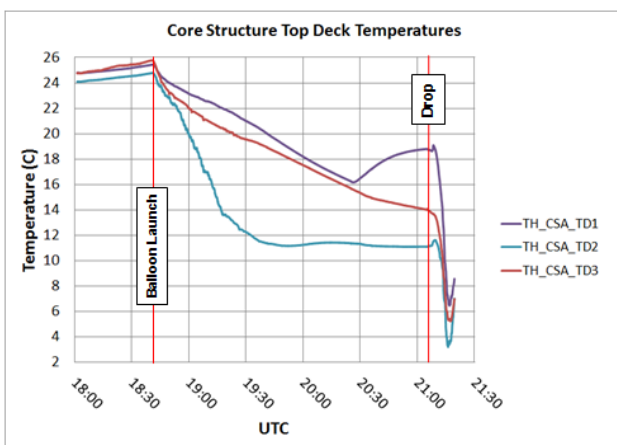


Figure 32. Core structure top deck outer facesheet temperatures.

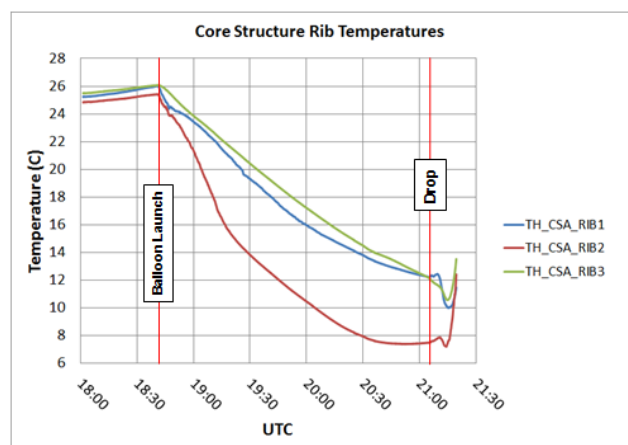


Figure 33. Core structure rib temperatures in vicinity of Star 48 Main Motor adaptor mounting ring.

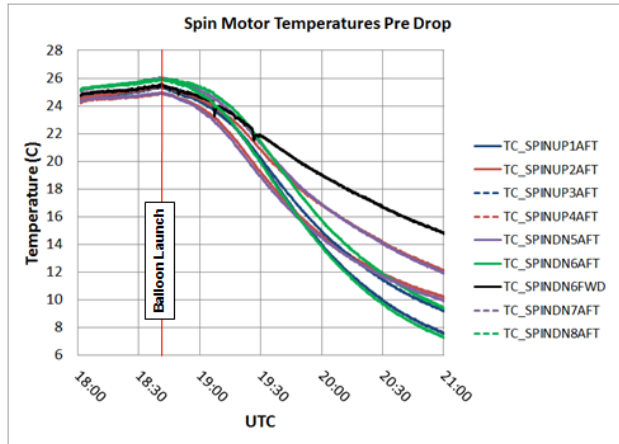


Figure 34. Spin Motor temperatures Pre Drop.

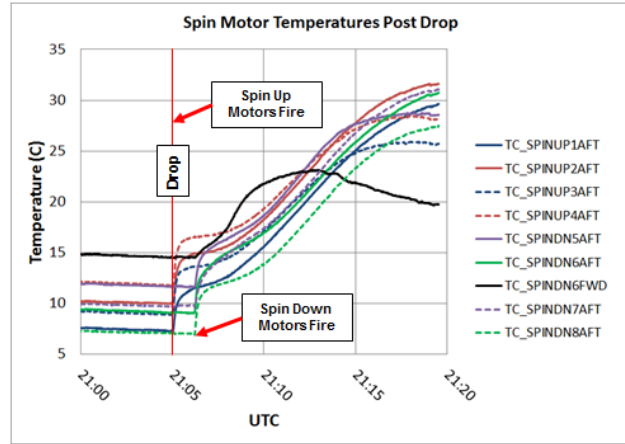


Figure 35. Spin Motor temperatures Post Drop.

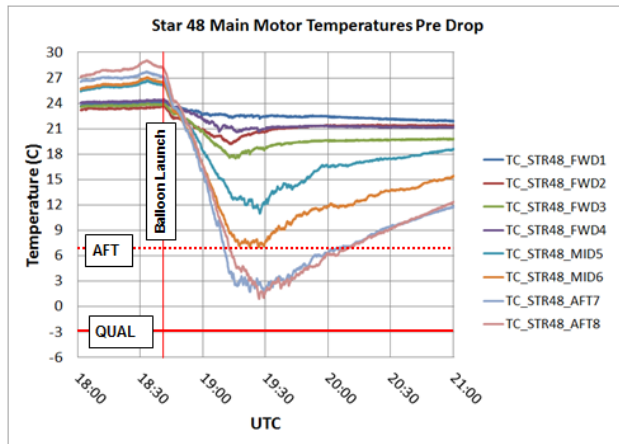


Figure 36. Star 48 Main Motor temperatures Pre Drop. AFT violation observed near nozzle during ascent.

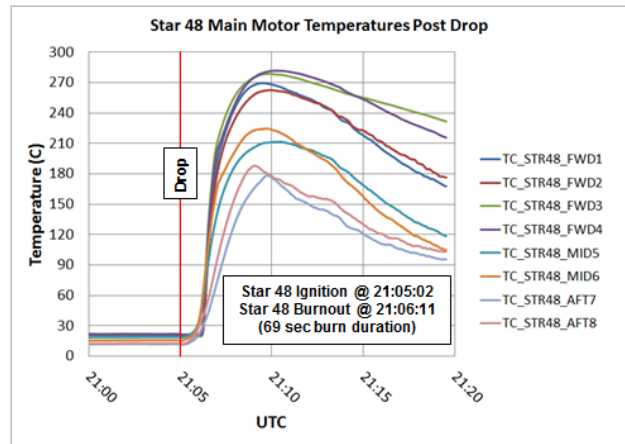


Figure 37. Star 48 Main Motor experienced soak back heating post engine burn up to a peak temp of 282°C.

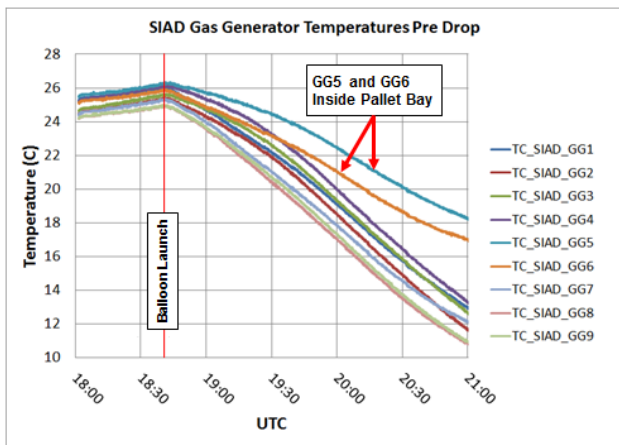


Figure 38. SIAD Gas Generator temperatures Pre Drop with GG5 and GG6 located inside the warmer pallet bay.

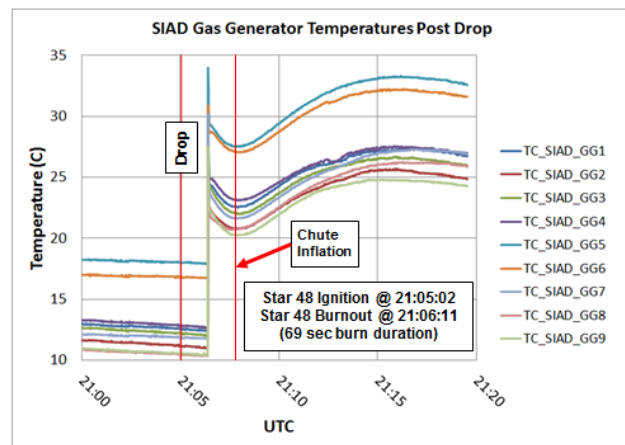


Figure 39. SIAD Gas Generator temperatures Post Drop.

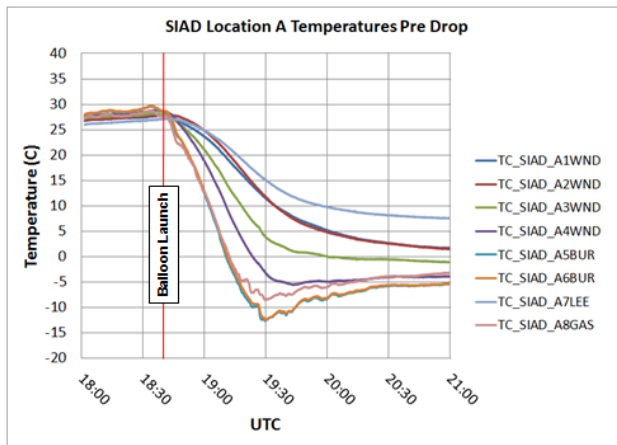


Figure 40. SIAD radial location A temperatures Pre Drop.

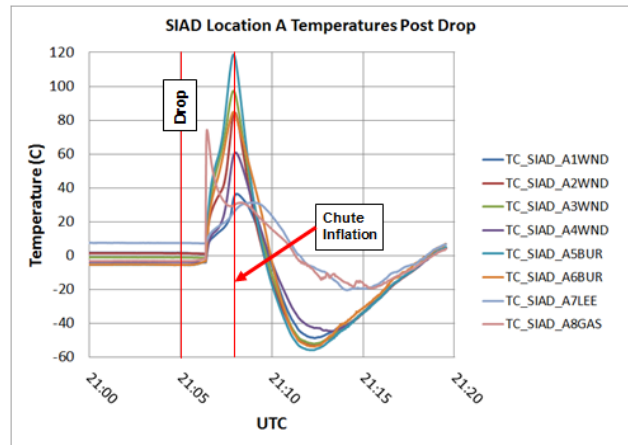


Figure 41. SIAD radial location A temperatures Post Drop.

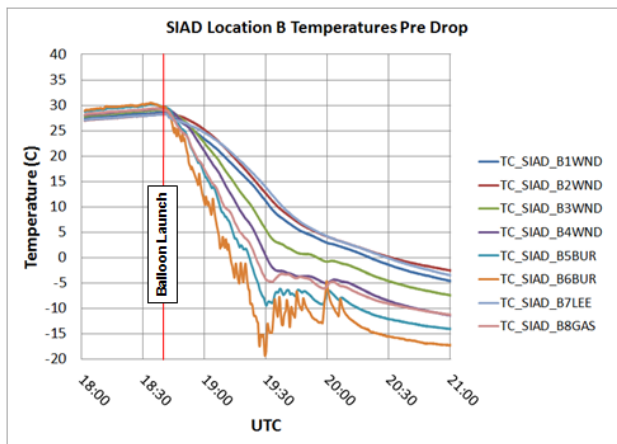


Figure 42. SIAD radial location B temperatures Pre Drop.

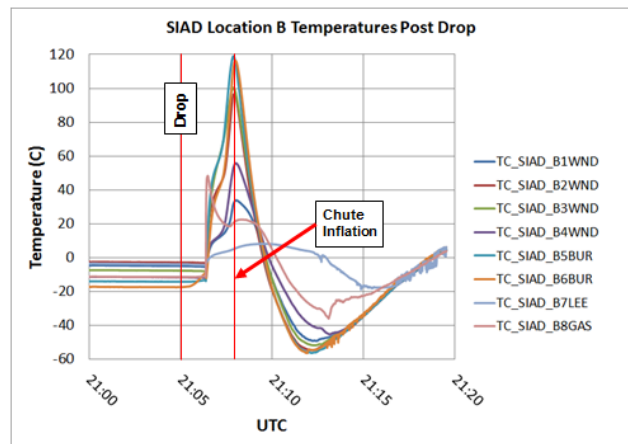


Figure 43. SIAD radial location B temperatures Post Drop.

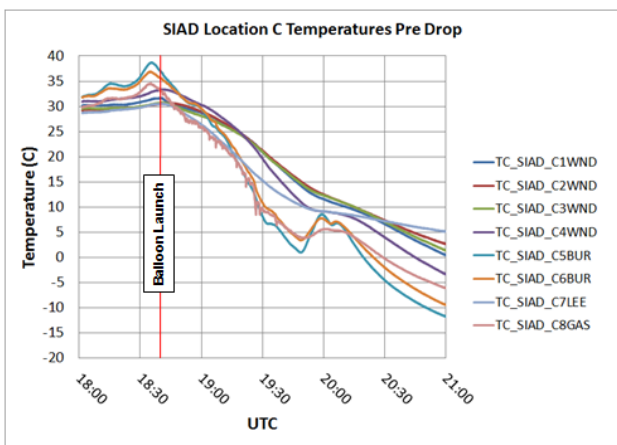


Figure 44. SIAD radial location C temperatures Pre Drop.

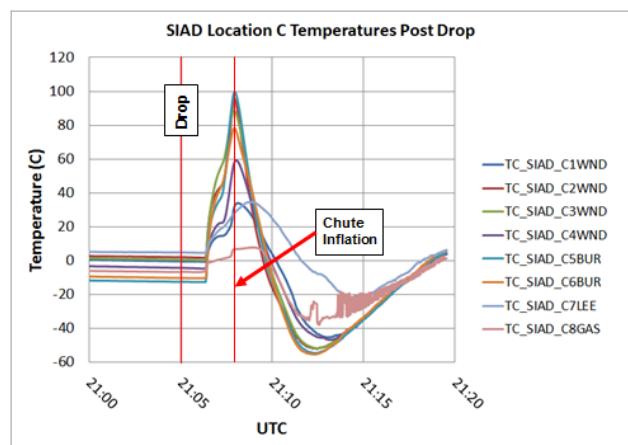
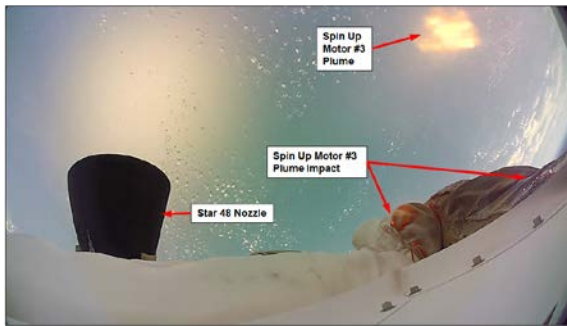


Figure 45. SIAD radial location C temperatures Post Drop.

considered a bit too benign for the SIAD and may be reconciled by the fact that the vehicle was lofted slightly higher than anticipated by the Star 48 Motor into a less dense regime where the aeroheating rates were lower than they should have nominally been. The highest temperatures were consistently recorded at *TC\_SIAD\_5BUR* locations, which is located on the windward side of the burble fence as shown in Fig. 14. This region was predicted to experience some of the highest heating rates<sup>13</sup>.

## VI. Post-Flight Visual TPS Inspection on the Recovered TV



**Figure 46. Regions of backshell TPS glowing hot with small flames after firing of Spin Up Motor.**

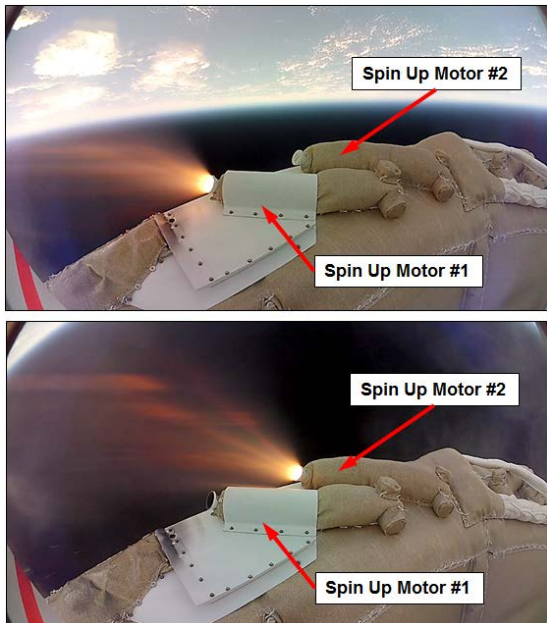


**Figure 47. Spin Up Motor #1 firing followed by Spin Up Motor #2 firing as viewed from Situational Video Camera #3.**

Figures 46-51 show all the key events during the powered flight test in the order that they happened. Figures 52-54 shows some images taken of the recovered test vehicle post-flight and highlight the blackened areas of the TPS that likely experienced high heating either from Spin Motor or Main Motor plumes. The blast shields for the Spin Up Motors seemed to have markedly more blackened area and soot deposits than those for the Spin Down Motors. This can likely be attributed to the fact that Spin Down Motor plumes occurred at a much higher altitude where the plumes themselves were allowed to widen more and become less concentrated in the lower density environment. Furthermore, there was no particle erosion observed whatsoever. Fears of this concern led to thicker than necessary shields being implemented. The cork Heat Shield showed no signs of charring or ablation, nor did a Teflon WRA cover which protruded through the Heat Shield show any signs of melting confirming predictions. Not shown, however, is the TPS which was underneath the forward dome of the Main Motor. It did have considerable blackening but like the rest of the TPS, it did not exhibit any signs of burn through and only surface discoloration was observed. The camera mast was surprisingly uncovered in black soot except for the very top and no ablation from the Spin Motor plume impingement was observed on the cork that encapsulated the FIR as was feared.

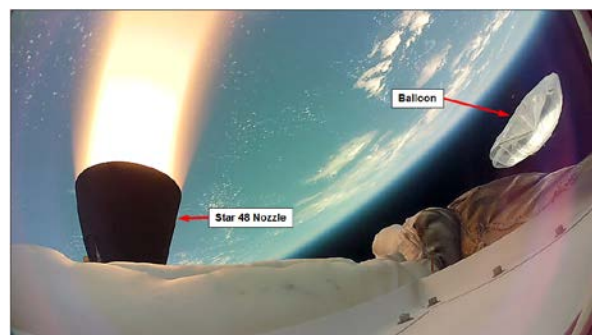


**Figure 48. Main Motor firing with detached carrier balloon in background.**

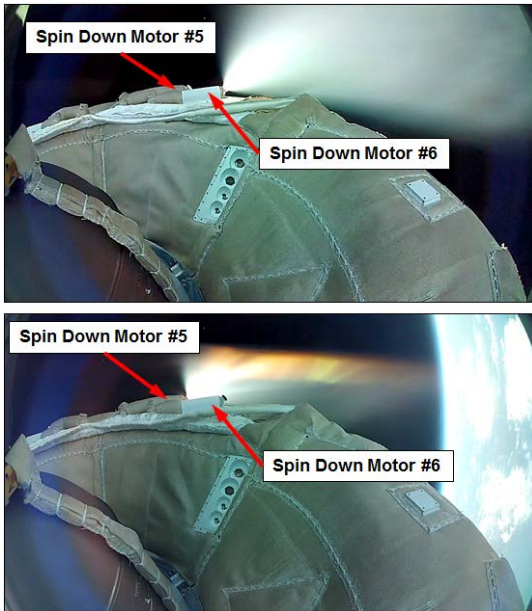


Figure 49. Spin Down Motor #6 firing followed by Spin Down Motor #5 firing as viewed from Situational Video Camera #2.

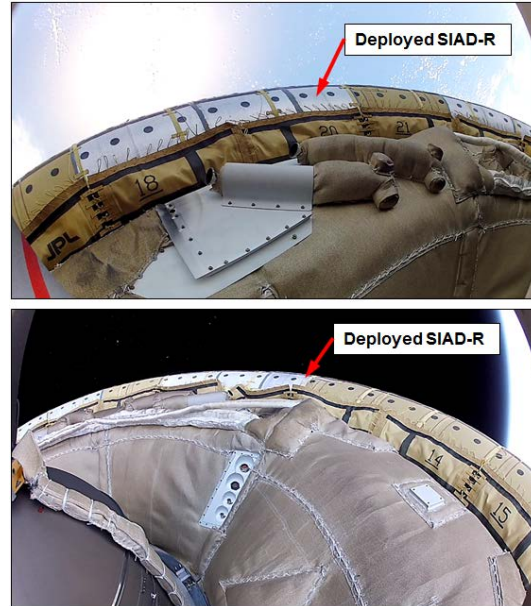


Figure 50. Successful SIAD-R deployment as viewed from the Situational Video Cameras.

## VII. Lessons Learned

It was very difficult to predict exactly what the thermal performance of the vehicle was going to be for the first test flight. Because this was a technology development test with very limited funding, no system level thermal vacuum test was scoped to help correlate the thermal model a priori, and the 4 major challenges revolving around the motor firing events had to be very conservatively estimated in order to guarantee that the vehicle thermal design would be robust. While it appears that the ascent and float environments were not completely bounded, many of the intrinsic thermal design features implemented just to survive the powered flight segment likely helped to provide additional insurance against those mission phases.

Since the powered flight segment became such a thermal design driver, there was a coarse plan in place to assess the true heating environments during SFDT-1. A number of stickers that were supposed to change color depending upon the temperature limits they reached were positioned in critical areas around the vehicle. Unfortunately, they didn't appear to register correctly when reviewed after the recovery. Immersion in salt water may have contaminated the actual results. So it is difficult to say with certainty just how conservative the Main Motor and Spin Motor plume heating was in reality. The Main Motor soakback heating, however, appears to have been too conservatively estimated, and sufficient telemetry now exists to provide a more refined estimate of it.

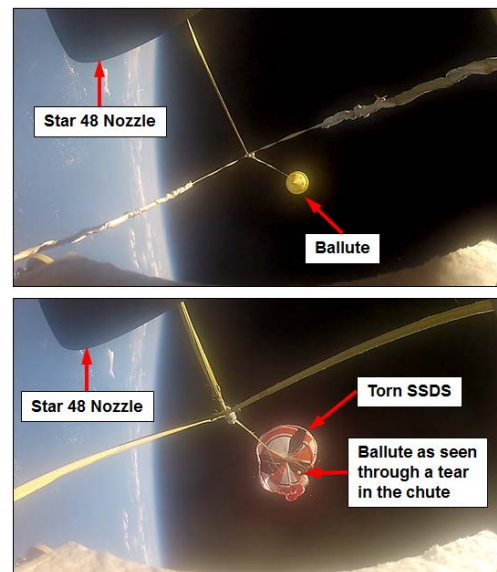


Figure 51. Successful ballute deployment followed by an unsuccessful chute deployment as viewed from the Situational Video Camera #4.

The Main Motor soakback heating, however, appears to have been too conservatively estimated, and sufficient telemetry now exists to provide a more refined estimate of it.



Figure 52. Recovered test vehicle showing Heat Shield (image on right) damaged from high speed water impact. Both the Heat Shield and the Teflon Water Recovery Aid (WRA) cover showed no signs of charring or melting.

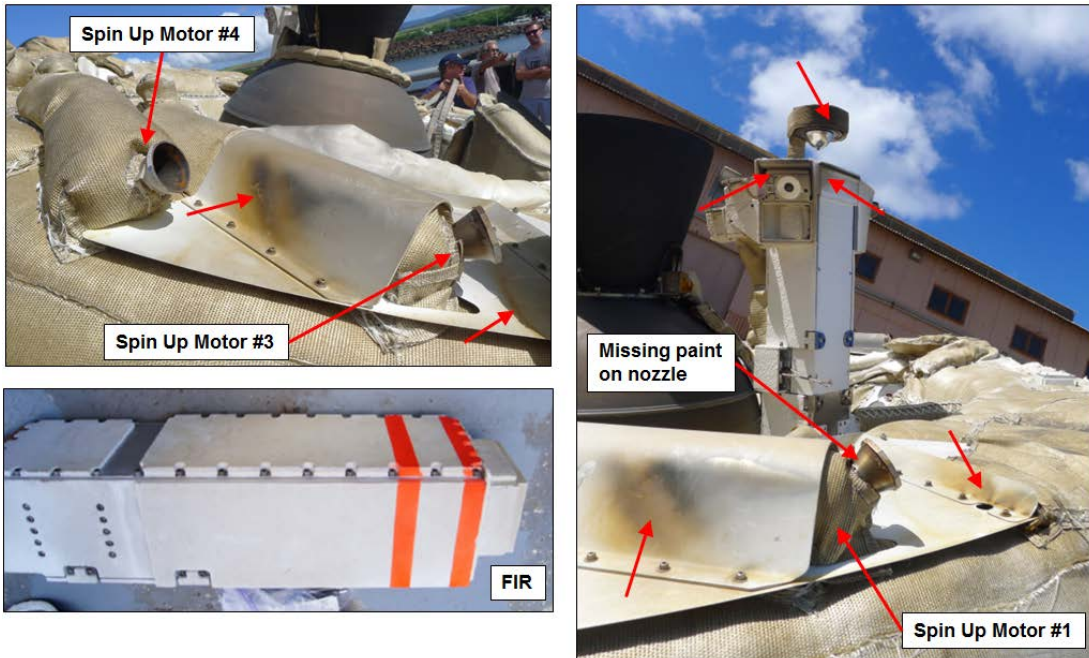
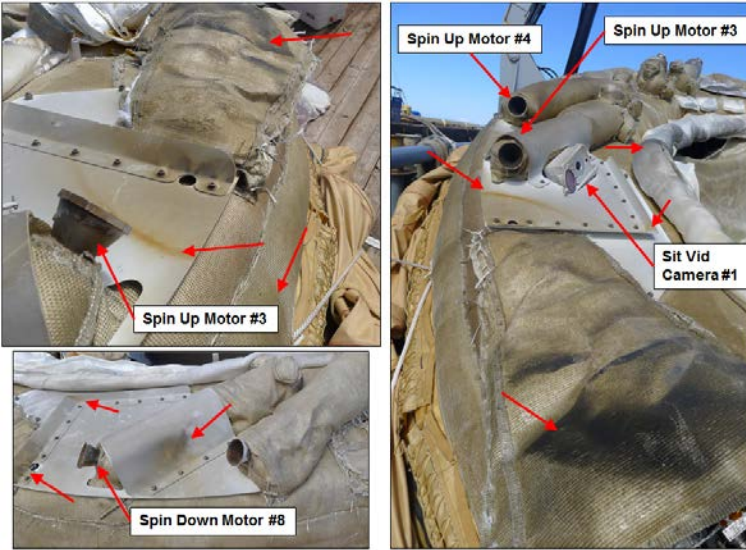


Figure 53. Unlabeled red arrows indicate areas where TPS was blackened due to plume heating. There was no significant particle erosion observed on the Spin Motor plume blast shields. While the FIR TPS had minor soot deposits, no ablation from the Spin Motor plumes was observed as was feared. The top of the camera mast had some noticeable soot deposits presumably from both the Spin Motor and Main Motor plumes.

## VIII. Conclusion

SFDT-1 was a highly successful test flight that met all stated objectives and goals. It can be safely declared that the thermal design of the vehicle was robust to the four major thermal challenges: the Star 48 Main Motor plume heating, the Star 48 Main Motor soakback heating, Spin Motor plume heating, and Spin Motor soakback heating. All components stayed well within AFTs except for the noted AFT violation observed near the nozzle end of the Star



**Figure 54. Unlabeled red arrows indicate areas where TPS was blackened due to plume heating. Spin Down Motor blast shields showed markedly less evidence of a high heating event as compared to the Spin Up Motors.**

48 Main Motor. The operations plan as executed worked flawlessly in terms of keeping the vehicle in a thermally safe condition throughout the entire mission timeline.

## Acknowledgments

The development described in this paper was carried out at the Jet Propulsion Laboratory, California Institute of Technology, under a contract with the National Aeronautics and Space Administration. The authors express their thanks to NASA's Office of the Chief Technologist for supporting this effort and enabling a select few to push the envelope. The authors wish to thank several of their colleagues at JPL who have been instrumental to the successful thermal performance of SFDT-1: Eric Sunada,

Sandria Gray, Brenda Hernandez, Brant Cook, Kevin Burke, John Luke Wolff, Gabriel Molina, Steven Schroeder, Jason Gates, Mark Duran, Richard Frisbee, Eric Oakes, George Chen, Grace Tan-Wang, Martin Greco, Steve Sell, Eric Blood, Marc Pomerantz, Thomas Randolph, Carl Guernsey, Mark Yerdon, Morgan Parker, Rebekah Tanimoto, Lou Giersch, John Gallon, Andrew Kennett, Coleman Richdale, Chris Tanner, Erich Brandeau, Paul Lytal, Ban Tieu, Chris Porter, and Rob Manning, as well as Virgil Mireles, Tony Paris, Pradeep Bhandari, and Bob Krylo for serving as the thermal review board members. The authors also wish to thank the following individuals from other NASA Centers including Brian Hall, Brian Abresch, Joel Simpson, Chris Purdy, Scott Hesh, Andrew Owens, Carl Davis, Michael Haugh, Jeff Benton, and Joe O'Brien from WFF and Brandon Mobley (MSFC), Bud Smith (MSFC) and Jay Grinstead (ARC) who provided critical inputs to the SFDT thermal model. Lastly, the authors would like to take this opportunity to acknowledge the LDSO project managers Mark Adler, Jeff Weis, and Principle Investigator, Ian Clark, for supporting the development of this paper.

## References

- <sup>1</sup>Moog, R., Bendura, R., Timmons, J. and Lau, R., "Qualification Flight Tests of the Viking Decelerator System," AIAA-1973-457, AIAA 4<sup>th</sup> Aerodynamic Deceleration Systems Conference, Palm Springs, California, May 1973.
- <sup>2</sup>Raper, J., Lundstrom, R. and Michel, F., "The Viking Parachute Qualification Test Technique," AIAA-1973-456, AIAA 4<sup>th</sup> Aerodynamic Deceleration Systems Conference, Palm Springs, California, May 1973.
- <sup>3</sup>Lundstrom, R., Raper, J., Bendura, R., and Shields, E., "Flight Tests of Viking Parachute System in Three Mach Number Regimes; I: Vehicle Description, Test Operations, and Performance," NASA Technical Note TN D-7692, October 1974.
- <sup>4</sup>Bendura, R.J., Lundstrom, R.R., Renfro, P.G., and LeCroy, S.R., "Flight Tests of Viking Parachute System in Three Mach Number Regimes II - Parachute Test Results," NASA Technical Note TN D-7734, pp. 1-96, 1974.
- <sup>5</sup>Buna, T., and Battley, H., "Thermal Design and Performance of the Viking Balloon-Launched Decelerator Test Vehicles," AIAA 1974-760, AIAA/ASME Thermophysics and Heat Transfer Conference, Boston, Massachusetts, July 1974.
- <sup>6</sup>NASA, "Fact Sheet: Low Density Supersonic Decelerators," [Online] JPL 400-1530, March 2013, <[http://www.nasa.gov/pdf/737628main\\_Final\\_LDSO\\_Fact\\_Sheet\\_3-26-13.pdf](http://www.nasa.gov/pdf/737628main_Final_LDSO_Fact_Sheet_3-26-13.pdf)>. [Accessed 07 April 2015].
- <sup>7</sup>NASA, "Press Kit: Low-Density Supersonic Decelerator (LDSO)," [Online] JPL 400-1530, May 2014, <[http://www.jpl.nasa.gov/news/press\\_kits/ldso.pdf](http://www.jpl.nasa.gov/news/press_kits/ldso.pdf)>. [Accessed 07 April 2015].
- <sup>8</sup>Cook, B., Blando, G., Kennett, A., Von Der Heydt, M., Wolff, J., and Yerdon, M., "High Altitude Supersonic Decelerator Test Vehicle," 22<sup>nd</sup> AIAA Aerodynamic Decelerator Systems Conference, Daytona Beach, Florida, March 2013.

<sup>9</sup>Smith, B.P., Tanner, C.L., Mahzari, M., Clark, I.G., Braun, R.D., and Cheatwood, F.M., "*A Historical Review of Inflatable Aerodynamic Decelerator Technology Development*," IEEE Aerospace Conference, Big Sky, MT, 2010.

<sup>10</sup>Giersch, L., Rivellini, T., Clark, I., Shook, L., Ware, J., and Welch, J., "*SIAD-R: A Supersonic Inflatable Aerodynamic Decelerator for Robotic missions to Mars*," 22<sup>nd</sup> AIAA Aerodynamic Decelerator Systems Conference, Daytona Beach, Florida, March 2013.

<sup>11</sup>Coatta, D., Jurewicz, D., Tutt, B., Rivellini, T., and Clark, I., "*Development and Testing of an 8 Meter Isotensoid Supersonic Inflatable Aerodynamic Decelerator*," 22<sup>nd</sup> AIAA Aerodynamic Decelerator Systems Conference, Daytona Beach, Florida, March 2013.

<sup>12</sup>Gallon, J.C., Clark, I.G., Rivellini, T.P., Adams, D.S., and Witkowski, A., "*Low Density Supersonic Decelerator Parachute Decelerator System*," AIAA Aerodynamic Decelerator Systems Conference, Daytona Beach, FL, 2013.

<sup>13</sup>Clark, I., and Blood, E., "*Low Density Supersonic Decelerator (LSD) Supersonic Flight Dynamics Test-1 (SFDT-1) Post-Test Report*," JPL Internal Document, D-81940, December 2014.

<sup>14</sup>Mastropietro, A. J., Pauken, M., Sunada, E., and Gray, S., "*Thermal Design and Analysis of the Supersonic Flight Dynamics Test Vehicle for the Low Density Supersonic Decelerator Project*," AIAA-2013-3348, 43<sup>rd</sup> International Conference on Environmental Systems, Vail, CO, 2013.

<sup>15</sup>Redmond, M., Mastropietro, A. J., Pauken, M., and Mobley, B., "*Passive Thermal Control for the Low Density Supersonic Decelerator (LSD) Test Vehicle Spin Motors Sub-System*," ICES-2014-031, 44<sup>th</sup> International Conference on Environmental Systems, Tucson, AZ, 2014.

<sup>16</sup>Redmond, M., and Mastropietro, A. J., "*Thermophysical and Optical Properties of Materials Considered for use on the LSD Test Vehicle*," ICES-2015-024, 45<sup>th</sup> International Conference on Environmental Systems, Bellevue, WA, 2015.